



HAL
open science

CRDS measurements of air-broadened lines in the 1.6 μm band of 12 CO 2: Line shape parameters with their temperature dependence

D. Mondelain, A. Campargue, H. Fleurbaey, S. Kassi, S. Vasilchenko

► To cite this version:

D. Mondelain, A. Campargue, H. Fleurbaey, S. Kassi, S. Vasilchenko. CRDS measurements of air-broadened lines in the 1.6 μm band of 12 CO 2: Line shape parameters with their temperature dependence. *Journal of Quantitative Spectroscopy and Radiative Transfer*, 2022, 288, pp.108267. 10.1016/j.jqsrt.2022.108267 . hal-03865630

HAL Id: hal-03865630

<https://hal.science/hal-03865630>

Submitted on 22 Nov 2022

HAL is a multi-disciplinary open access archive for the deposit and dissemination of scientific research documents, whether they are published or not. The documents may come from teaching and research institutions in France or abroad, or from public or private research centers.

L'archive ouverte pluridisciplinaire **HAL**, est destinée au dépôt et à la diffusion de documents scientifiques de niveau recherche, publiés ou non, émanant des établissements d'enseignement et de recherche français ou étrangers, des laboratoires publics ou privés.

1 **CRDS measurements of air-broadened lines in the 1.6 μm band of $^{12}\text{CO}_2$:**
2 **Line shape parameters with their temperature dependence**

3
4
5 D. Mondelain*, A. Campargue, H. Fleurbaey, S. Kassi, S. Vasilchenko

6
7 *Univ. Grenoble Alpes, CNRS, LIPhy, 38000 Grenoble, France*

8
9
10
11
12 *Corresponding author: didier.mondelain@univ-grenoble-alpes.fr; LIPhy, Bat. E, 140 rue de la
13 Physique, 38400 Saint-Martin d'Hères (France).

14
15
16
17
18
19
20
21
22 **Key words**

23 Line shape; carbon dioxide; temperature dependence; CRDS

24

25 **Abstract**

26 The $^{12}\text{CO}_2$ band at 1.6 μm is used for carbon dioxide monitoring in the Earth atmosphere. The
27 targeted accuracy of these measurements motivates important efforts to improve the quality of the
28 spectroscopic parameters in atmospheric conditions. In the present work, the line shapes of the R(6),
29 R(12), R(16), R(18) and R(20) transitions of the 30013-00001 band of $^{12}\text{CO}_2$ in air are studied with a
30 cavity ring down spectrometer (CRDS). For each transition, high signal-to-noise ratio spectra
31 (between 2000 and 20000) are recorded at different temperatures (250, 274, 285, 295 and 320 K)
32 and total pressures (50, 100, 250, 500 and 750 Torr). To this end, a spectrally narrowed and stable
33 (sub-kHz) laser source is coupled into a temperature regulated high-finesse optical cavity. The
34 frequency scale of each spectrum is accurately determined from measurements of the frequency of
35 the beat note between a part of the laser light and the closest tooth of a frequency comb referenced
36 to a rubidium clock. A multi-spectrum fit procedure with quadratic speed dependent Nelkin-Ghatak
37 profiles, including line-mixing effects, has been used to derive for each transition, the different
38 spectroscopic parameters and their temperature dependence. Results are discussed in comparison
39 with previous experimental data, HITRAN2020 database and values obtained from requantized
40 classical molecular dynamics simulations (rCMDS).

41

42 **1. Introduction**

43 Due to its importance for remote sensing applications from ground- or satellite-based
44 observatories, the 30013-00001 band of $^{12}\text{CO}_2$ in the 1.6 μm atmospheric transparency window has
45 been the subject of many laboratory studies using Fourier transform spectroscopy (FTS) [1,2 and
46 references herein] and cavity ring down spectroscopy (CRDS) [3,4,5,6,7]. This band is especially used
47 to monitor the column averaged CO_2 atmospheric dry air mole fraction, X_{CO_2} , in several satellite
48 missions like the Orbiting Carbon Observatory-2 (OCO-2) [8,9,10], OCO-3 [11] and GOSAT [12]. A
49 relative uncertainty of less than 0.3 % (*i.e.* ~ 1 ppm) is required [13] to better characterize the surface
50 CO_2 sources and sinks on regional scales and constrain the climate models. This brings strong quality
51 constraints on the spectroscopic parameters which have to be determined with very small
52 uncertainties. As stated in [14], *the spectroscopic error estimates (...) are generally comparable to or*
53 *larger than the noise-only X_{CO_2} posterior uncertainty (...)*, showing the importance of new
54 experimental data with improved accuracy. Moreover, upcoming missions like CO2M [15] will have
55 even stronger requirements on X_{CO_2} and thus on the spectroscopic parameters and their temperature
56 dependence. In parallel, it is necessary to make available accurate spectroscopic line-shape
57 parameters for CO_2 lines to improve the semi-empirical models used to update all of the carbon
58 dioxide transitions in the spectroscopic databases (*e.g.* HITRAN [16] or GEISA [17]), especially for the
59 non-Voigt parameters [18]. The same accurate experimental data are also valuable for validation
60 tests of the parameters provided by requantized classical molecular dynamics simulations (rCMDS)
61 [19].

62 The aim of this work is to determine the line-shape parameters and their temperature
63 dependence with a reduced uncertainty for five transitions belonging to the R-branch of the 30013-
64 00001 band of $^{12}\text{CO}_2$ in air. To achieve this goal, parameters are retrieved from high signal-to-noise
65 ratio CRDS spectra recorded at different temperature and pressure conditions with a spectrally
66 narrowed and stable (sub-kHz) laser source coupled into a temperature regulated high-finesse
67 optical cavity. The frequency scale of each spectrum is accurately determined from measurements of
68 the frequency of the beat note between a part of the laser light and the closest tooth of a frequency
69 comb referenced to a rubidium clock. The experimental set-up is described in Part 2 together with
70 the recording procedure. The multi-spectrum fit procedure and the retrieved spectroscopic
71 parameters are detailed in Part 3. The latter are compared with the most recent and accurate
72 experimental and theoretical data in Part 4 before concluding (Part 5).

73

74 2. Experimental details

75 2.1 The setup

76 The comb-referenced cavity ring down spectrometer used for the recordings has been detailed in
77 [20] and is only briefly described here. The light source consists in a distributed feedback (DFB) laser
78 diode narrowed to sub-kHz level thanks to an optical feedback signal from a stable V-shape high
79 finesse cavity (FSR= 480 MHz; finesse= 500000) made of ultra-low expansion glass [21]. At the same
80 time, the optical feedback allows locking the laser diode to one of the longitudinal cavity modes. The
81 continuous tuning of the light source is achieved thanks to a Mach-Zehnder modulator (MZM)
82 generating a side-band scanned between 2 GHz and 22 GHz from the carrier frequency (*i.e.* over 0.67
83 cm^{-1}). By locking the laser diode to different cavity modes and changing the side band frequency, a
84 continuous tuning is achieved between 6231.5 cm^{-1} and 6243.5 cm^{-1} with the DFB diode at disposal
85 (From Fitel). Due to the low efficiency ($\sim 5\%$) of the MZM, the output beam is amplified by a booster
86 optical amplifier (BOA) before being separated in three parts: towards the high finesse cavity, the
87 wavelength meter (HighFinesse WSU7-IR) and the frequency comb (Model FC 1500-250 WG from
88 Menlo Systems).

89 Most of the light is coupled into a temperature stabilized high finesse cavity (TS-HFC) described in
90 [22] where ring down (RD) events are achieved at resonance by switching the laser light off with an
91 acousto-optic modulator (AOM). The extinction coefficient, $\alpha(\nu)$, is deduced from:

$$92 \quad \alpha(\nu) = \frac{n}{c\tau(\nu)} - \frac{1}{c\tau_0(\nu)} \quad (1)$$

93 where τ and τ_0 are the RD times for the cell filled with the gas mixture and evacuated, respectively, c
94 is the speed of light and n is the refractive index of the absorbing gas. RD events are acquired at a
95 typical rate of 200 RD/s by applying a triangular voltage ramp coupled to a RD tracking loop on the
96 PZT tube on which the output cavity mirror is mounted [20].

97 Accurate measurement of the absolute frequency of the laser source is deduced at each RD event
98 from the frequency of the beat note, f_{BN} , between a part of the light source and one tooth of a
99 frequency comb (FC) [20]. The comb tooth number is determined from the wavelength meter
100 measurements.

101 Two versions of the TS-HFC, described in [20] and [22], are used here, namely the V1 (FSR= 258
102 MHz; $F \sim 211600$) and the improved V2 (FSR= 332 MHz; $F \sim 310600$) versions. Both work on the same
103 principle (see Fig.1 of Ref. [22]): a fluid, whose temperature is regulated using a deported
104 refrigerated/heating circulator (model Corio 1000F from Julabo), flows through two counter-
105 propagating copper coils wrapped around a tube containing the two dielectric mirrors of the cavity.
106 An inner copper tube is placed between the mirrors to limit the convection and reduce exchange of
107 the gas inside the tube with the surrounding gas. It has been shown that the surrounded gas is very

108 well thermalized to the tube temperature (with a difference smaller than 0.05°C) [20]. The latter is
 109 measured by four 3-wires 1000 Ω platinum temperature sensors (⅓ DIN class B; accuracy: ±0.1 K to
 110 0.2 K) for the V1 cell and by five 4-wires 100 Ω platinum temperature sensors (class 1/10 DIN) giving
 111 an accuracy equal to 0.03+0.0005*t* (with *t* the temperature in °C) for the V2 cell. In both versions, the
 112 gas temperature can be regulated over the 245-330 K range, with a maximal temperature variation
 113 along the inner tube, Δ*T*, of 0.5 K and 0.1 K for the for the V1 and V2 cell, respectively. The former
 114 one was used for spectra recordings at room temperature and 274 K, where Δ*T* is kept below 0.3 K,
 115 and the latter one at 320, 285 and 250 K (**Table 1**). The temperature variations are limited to only
 116 0.04 K over ~14h at 250 K.

117 A gas mixture of 398.9±2.0 (2σ) mol-ppm of CO₂ in air (Ar: ~1 mol-% ; O₂: ~20.95 mol-%; N₂: ~
 118 78.05 mol-%) provided by AirLiquide is used in this work. The pressure in the cells is measured by a
 119 heated absolute Baratron capacitance manometer (1000 mbar full scale; accuracy: 0.10% of reading).

30013-00001	ν_0 cm ⁻¹	$S(296\text{ K})$ cm/mol	320K	295K	285K	274K	250K
R(6)	6233.183	1.097×10 ⁻²³	V2	V1	V2	V1	V2
R(12)	6237.421	1.656×10 ⁻²³	V2	V1	V2	V1	V2
R(16)	6240.104	1.751×10 ⁻²³	V2	V1	V2	V1	V2
R(18)	6241.403	1.721×10 ⁻²³	V2	V1	V2	V1	V2
R(20)	6242.672	1.646×10 ⁻²³	V2	V1	V2	V1	V2

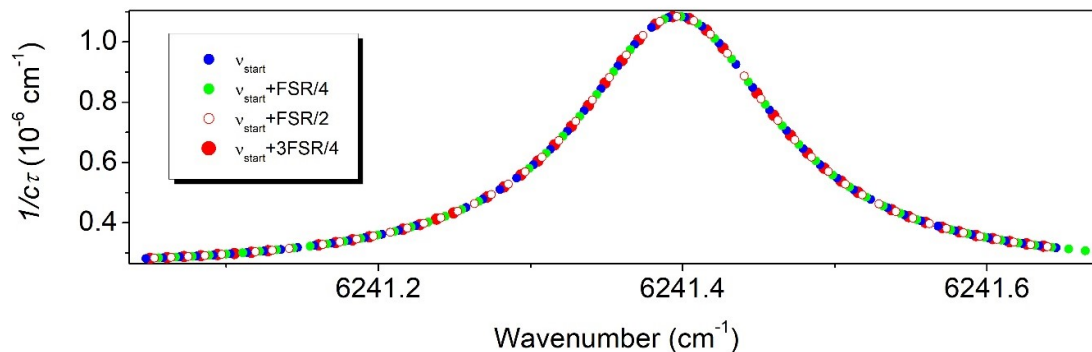
120
 121 *Table 1. Summary of the temperature conditions and cell version used to record the five CO₂ transitions studied*
 122 *in this work. Position and intensity values are those provided in the HITRAN database [16].*

123

124 2.2. Spectra acquisition

125 For each transition and temperature conditions reported in **Table 1**, a series of spectra are
 126 recorded for five total pressure values (750, 500, 250, 100 and 50 Torr). With the V1 cell, one
 127 spectrum was recorded for each pressure with a sampling step corresponding to the FSR of the cavity
 128 (*i.e.* 0.0087 cm⁻¹). The spectral sampling corresponding to the FSR of the cavity is adopted to increase
 129 the efficiency of the RD tracking loop (reducing the acquisition time) as the resonance always occurs
 130 at the same offset value of the ramp. With V2, the recording procedure was modified to provide
 131 more measurement points: at each pressure, four spectra were recorded for the absorption line from
 132 the starting frequency, f_{start} , for the first one and from f_{start} shifted by ¼, ½ and ¾ of the FSR value for
 133 the others (**Figure 1**). The acquisition time of one spectrum is typically 1 to 2 minutes. It is important
 134 to mention that as the CO₂ concentration can slightly evolve with time due to adsorption or
 135 desorption on the walls of the cell, it is a better choice to not concatenate the spectra recorded at a
 136 given pressure but fit them separately during the multi-spectrum fitting procedure described below.
 137 In this way, the evolution of the concentration over one spectrum can be considered as negligible

138 (0.1% in the worst case). Note that the adsorption or desorption rate depends on the temperature
139 and pressure conditions.



140

141 *Figure 1. The spectral sampling applied during the spectra recordings with V2 of the TS-HFC illustrated here*
142 *for the R(18) transition at 750 Torr and 250 K with the CO₂ in air mixture. The different colors correspond to the*
143 *four interlaced spectra.*

144 During the spectra recordings, an adaptative averaging procedure is applied to compensate the
145 noise level increase occurring at strong absorption near the center of the lines. This consists in
146 automatically increasing the number of RDs averaged per spectral point with absorption until a user
147 defined maximum value (in order to avoid too long acquisition times). Typically, 50 and 250 RD
148 events are averaged in the wings and at the top of the absorption line, respectively.

149 3. Line profile analysis

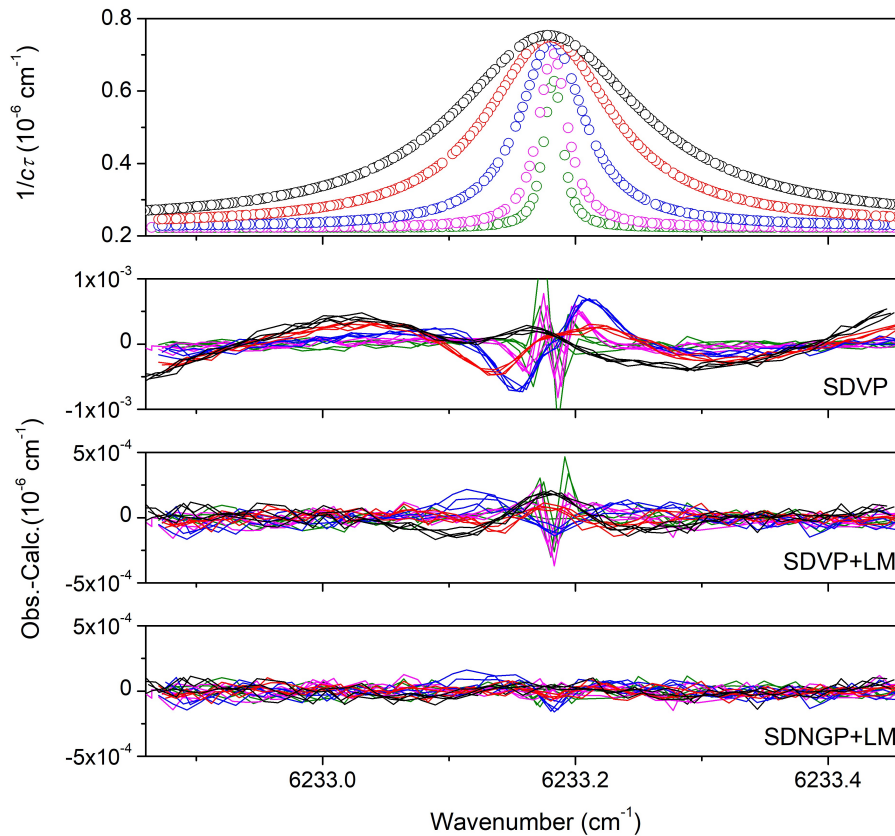
150 3.1. The multi-spectrum fit procedure

151 The same fit procedure is adopted for all the transitions: at a given temperature the five (V1 cell)
152 or twenty spectra (corresponding to the four interlaced spectra times the five pressures in the case
153 of the V2 cell) are taken into account in a multi-spectrum fit procedure using the *Multi-spectrum*
154 *Analysis Tool for Spectroscopy (MATS)* fitting program [23] developed at NIST. As illustrated in **Figure**
155 **2**. Large residuals are obtained if the speed dependent Voigt profile is used. A better spectra
156 reproduction is achieved by adding line-mixing effects but to reduce residuals at the noise level, it is
157 necessary to use a speed-dependent Nelkin-Ghatak profile (SDNGP) [24] including first-order line
158 mixing [25]. Note that the first-order approximation adopted in our work is valid if the off-diagonal
159 relaxation matrix element coefficients times the pressure is much smaller than the difference
160 between the positions of the neighbor lines [18]. This condition is verified in our case with matrix
161 element coefficients smaller than 0.025 cm⁻¹atm⁻¹ [1] and differences in position on the order of ~1.3
162 cm⁻¹ and maximum pressure values of 1 atm. The SDNG profile takes into account the Doppler effect,
163 the collision-induced velocity changes, quantified by the velocity changing collision rate (in cm⁻¹), ν_{VC} ,
164 the collisional broadening and shift for which a quadratic law is used for the speed dependence such
165 that:

166
$$\Gamma(\nu) = \Gamma_0 + \Gamma_2 \left[\left(\frac{\nu}{\tilde{\nu}} \right)^2 - 3/2 \right] \quad (2)$$

167 and
$$\Delta(\nu) = \Delta_0 + \Delta_2 \left[\left(\frac{\nu}{\tilde{\nu}} \right)^2 - 3/2 \right] \quad (3)$$

168 where Γ_0 and Δ_0 (in cm^{-1}) correspond to the (thermally averaged) line width and shift, respectively,
 169 and Γ_2 and Δ_2 (in cm^{-1}) are the speed dependence components. $\tilde{\nu} = \sqrt{\frac{2k_B T}{m}}$ is the most probable
 170 speed of the absorbing molecule ($^{12}\text{C}^{16}\text{O}_2$) of mass m . The first-order line mixing is characterized by
 171 the dimensionless Y parameter. Note that when fitting the correlation parameter, η , with a
 172 Hartmann Tran profile (HTP), the retrieved value is close to 0 and does not improve the fit quality.
 173 Thus, to avoid the risk of a overfitting of the spectra [26], we decided to fix η to 0 corresponding to a
 174 SDNG profile.



175
 176 *Figure 2. Series of CRDS spectra recorded for the R(6) transition at 250 K for five pressures between 50 and*
 177 *750 Torr (upper panel). Corresponding fit residuals (exp-fit) obtained after the multi-spectrum fit procedure with*
 178 *different line profiles are shown on the lower panels. The different colors correspond to the different pressures.*
 179 *For each pressure value, the residuals of the four interlaced spectra are displayed. The quality factors vary*
 180 *between 7700 and 14300 according to the spectrum in the case of SDNGP+LM. Note the different y-scales on*
 181 *the residuals.*

182 In the multi-spectrum fit procedure, the wavenumber of the spectral line at zero pressure, ν_0 , the
 183 line-broadening and pressure-shift coefficients γ_0 (Γ_0/P , in $\text{cm}^{-1}\text{atm}^{-1}$) and δ_0 (Δ_0/P , in $\text{cm}^{-1}\text{atm}^{-1}$), their
 184 speed dependence components γ_2 (Γ_2/P , in $\text{cm}^{-1}\text{atm}^{-1}$) and δ_2 (Δ_2/P , in $\text{cm}^{-1}\text{atm}^{-1}$), the Dicke
 185 narrowing parameter β (ν_{vc}/P , in $\text{cm}^{-1}\text{atm}^{-1}$) and the first-order line-mixing coefficient ζ (Y/P , in atm^{-1})
 186 are globally fitted for each temperature. The mixing ratio of CO_2 , X_{CO_2} , is fixed to the value of 398.9
 187 ppm given by the gas supplier. The Doppler width is fixed to its calculated value at the measured
 188 temperature and the line intensity, S , and the linear baseline are fitted independently for each
 189 spectrum. As shown on **Figure 2** for the R(6) transition at 250 K, residuals at the noise level (which is
 190 typically $5 \times 10^{-11} \text{ cm}^{-1}$ in this case) are achieved using the multi-spectrum fit procedure and
 191 SDNGP+LM. This leads to quality factors between 7700 and 14300 in this case (QF is defined as the
 192 ratio of the absorption at the peak to the *rms* of the residuals).

193 It is important to mention that, during the fit procedure, the absorption due to the weak CO_2 lines
 194 in the neighbourhood of the fitted transition is taken into account by the *MATS* program based on
 195 the HITRAN2020 database [16] using a Voigt profile and $X_{\text{CO}_2}=398.9$ ppm. If significant, absorption
 196 due to the interfering water vapour transitions is also calculated and included in the simulation, using
 197 the same database and a concentration fixed to a value deduced from isolated H_2O lines. Water
 198 vapour mixing ratios were found to be lower than 140 ppm.

199 The parameter values of this multi-spectrum fit procedure are provided in Supplementary
 200 Material for each transition at the different temperatures.

201 3.2. Temperature dependence of the line parameters

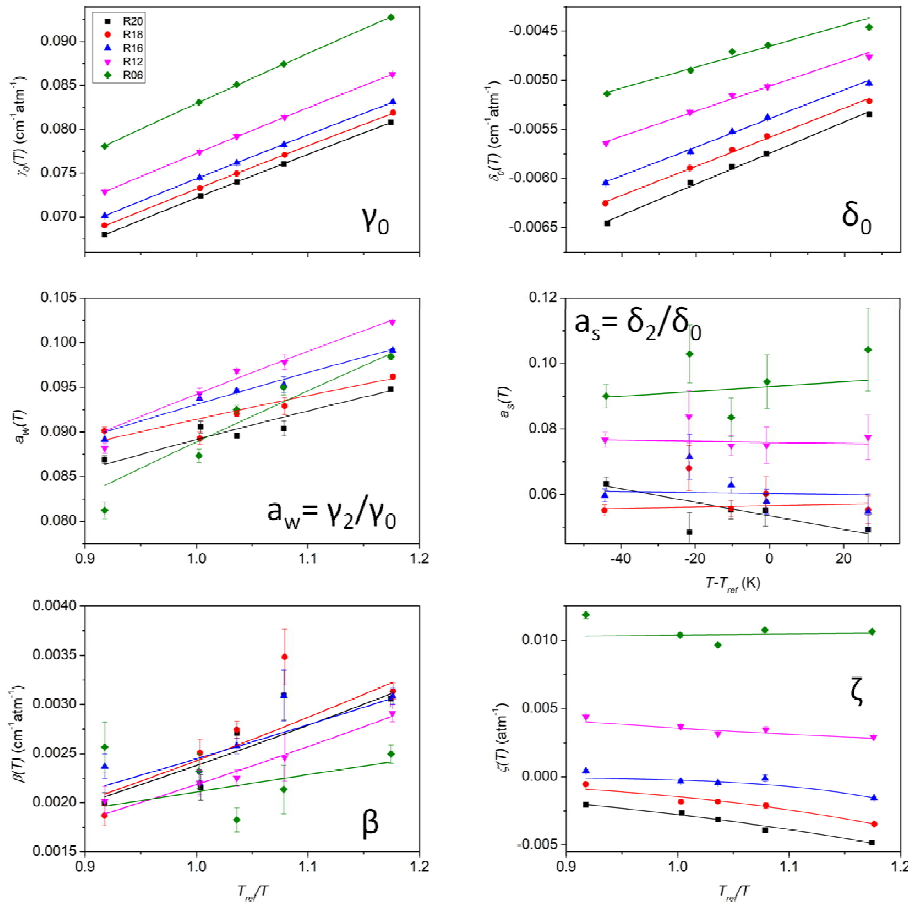
202 The multi-spectrum fit procedure applied to the five transitions provides sets of spectroscopic
 203 parameters for five temperatures between 250 and 320 K. The temperature dependence of the line
 204 parameters can be empirically modelled using the usual power law of the form: $A(T) =$

205 $A(T_{ref}) \left(\frac{T_{ref}}{T} \right)^{n_A}$ where $T_{ref} = 296$ K, $A(T)$ corresponds to either γ_0 , γ_2 , β or ζ and n_A is the

206 corresponding temperature dependence exponent. In the case of the pressure shift and its speed
 207 dependence component (δ_2), the following linear dependence is applied: $\delta_i(T) = \delta_i(T_{ref}) +$
 208 $\delta'_i(T - T_{ref})$ (with $i=0$ or 2) to allow for a change of sign for δ_i . Note that since we are working with
 209 a mixture of CO_2 at a very low mixing ratio in air ($X_{\text{CO}_2}=398.9$ ppm), the contribution due to collisions
 210 between two CO_2 molecules can be neglected for all parameters. For example, as $\gamma_0(T) =$
 211 $\gamma_{self}(T)X_{\text{CO}_2}P_{tot} + \gamma_{air}(T)(1 - X_{\text{CO}_2})P_{tot}$, γ_0 can be assimilated to γ_{air} with a relative error smaller
 212 than 1.5×10^{-4} .

213 Plotting the retrieved parameters $\gamma_0(T)$, $\beta(T)$ and $\zeta(T)$ versus T_{ref}/T and fitting these data points
 214 with a function of the form $y= ax^b$, allows determining $A(T_{ref})$ and n_A . In the same way, $\delta_0(T)$ is plotted
 215 versus $(T-T_{ref})$ to retrieve $\delta_0(T_{ref})$ and δ'_0 . In the case of $\gamma_2(T)$ the things are slightly different, as in the
 216 MATS program the fit output corresponds to $a_w = \frac{\gamma_2(T)}{\gamma_0(T_{ref})}$ because no temperature dependence is
 217 assumed *a priori* ($n_{\gamma_2} = 0$). Hence, by plotting $a_w(T)$ versus T_{ref}/T and fitting these data points with a
 218 function of the form $y=ax^b$ we obtain $a_w(T_{ref})= \gamma_2(T_{ref})/\gamma_0(T_{ref})$ and n_{γ_2} . In the case of $\delta_2(T)$, the fit
 219 output corresponds to $a_s = \frac{\delta_2(T)}{\delta_0(T_{ref})}$. By plotting a_s versus $(T-T_{ref})$, we obtain $a_s(T_{ref})= \delta_2(T_{ref})/\delta_0(T_{ref})$
 220 and δ'_2 .

221 The different parameters obtained from the multi-spectrum fit procedure are plotted versus
 222 temperature on **Figure 3**. The retrieved parameter values at T_{ref} and their temperature dependence
 223 coefficients are given in **Table 2** and compared with the most accurate literature data in the next
 224 section. Note that in the fits on **Figure 3**, the data are weighted by the inverse of the squared
 225 uncertainty estimated as discussed below.



226
 227 **Figure 3.** Variation of the fitted parameters of the R(6), R(12), R(16), R(18) and R(20) lines of the 30013-00001
 228 band of $^{12}\text{CO}_2$ versus the temperature. The parameters γ_0 , β , a_w , ζ are fitted with a function of the form $y= ax^b$ to

229 *determine their value at T_{ref} and the temperature dependence exponent. The δ_0 and a_s parameters are fitted*
230 *with a linear function which provides their value at T_{ref} and the temperature dependence coefficient (see text).*

231

	γ_0 $cm^{-1}atm^{-1}$	n_{γ_0}	δ_0 $cm^{-1}atm^{-1}$	δ' $cm^{-1}atm^{-1}K^{-1}$	β $cm^{-1}atm^{-1}$	n_β	a_w	n_{γ_2}	a_s^*	ζ atm^{-1}	n_ζ
R(6)	0.08295(3)	0.698(4)	-0.00465(3)	0.0000107(10)	0.00211(22)	0.8(9)	0.0889(12)	0.66(10)	0.093(5)	0.01040(49)	0.1(4)
R(12)	0.07726(1)	0.682(2)	-0.00506(2)	0.0000128(7)	0.00218(5)	1.7(2)	0.0942(6)	0.52(5)	0.076(2)	0.00357(15)	-1.4(4)
R(16)	0.07437(1)	0.683(2)	-0.00539(1)	0.0000146(5)	0.00245(10)	1.4(4)	0.0931(3)	0.39(3)	0.060(3)	-0.00024(12)	11.5(32)
R(18)	0.07318(3)	0.687(4)	-0.00558(1)	0.0000148(5)	0.00243(13)	1.8(5)	0.0914(5)	0.30(5)	0.057(2)	-0.00146(13)	5.4(6)
R(20)	0.07218(2)	0.699(3)	-0.00574(2)	0.0000158(6)	0.00238(11)	1.7(4)	0.0892(5)	0.37(4)	0.054(2)	-0.00277(6)	3.5(2)

232

233 *Note*

234 **These values correspond to the mean value averaged over all the temperatures.*

235 *Table 2. List of the spectroscopic parameters obtained for the five transitions studied in this work. A SDNG profile is used in the multi-spectrum fit procedure. One-sigma*
236 *uncertainties are given in parenthesis in the unit of the last digit. Here, a_w and a_s correspond to γ_2/γ_0 and δ_2/δ_0 , respectively.*

237 3.3 Estimated error budget

238 a. Type-A uncertainty

239 As explained in [26], the standard error provided for each fitted parameter by the *MATS* program
240 could underestimate the « real error » by factors between typically 3 to 5, depending of the
241 considered parameter, because the numerical correlations between the parameters are not taken
242 into account in the calculation of this standard error. To estimate these factors in our case, we first
243 simulated 100 spectra with different random noise and then calculated the standard deviation of the
244 fitted parameters. In our typical noise conditions (10 kHz or $\sigma_x = 3 \times 10^{-3}\%$ of the Doppler FWHM on the
245 x-axis and $1 \times 10^{-10} \text{ cm}^{-1}$ or $\sigma_y = 0.02\%$ of the maximum absorption on the y-axis), we found that the
246 uncertainty reported for the fitted parameters is equivalent to the « real error » showing that the
247 impact of the correlation between the parameters is small thanks to the low noise level on the two
248 axis. The fit errors are thus directly considered as our type-A uncertainty.

249 b. Type-B uncertainty

250 To evaluate possible biases due to inaccurate pressure and temperature values, we also adopted
251 the method described in [26] consisting, for a given transition and temperature, in: (i) generating a
252 set of spectra at the five pressures of the recordings using our list of spectroscopic parameters and a
253 SDNG profile and fixing one parameter (the temperature or the total pressure in our case) to its
254 biased value and, then (ii) fitting these simulated spectra with the « true » temperature or total
255 pressure. The retrieved spectroscopic parameters are then compared to the values used to generate
256 the spectra. Here we adopted a bias of 0.1% for the total pressure, corresponding to the uncertainty
257 of the pressure gauge, and a bias of 0.1 K for the temperature reflecting the uncertainty on the
258 absolute temperature measurement and the inhomogeneity of the sounded gas temperature [20]. At
259 274 K a bias of 0.3 K is applied due to the larger temperature inhomogeneity of the V1 cell. These
260 evaluations have been done for all the transitions and temperatures. Note that a bias related to X_{CO_2}
261 was not considered here as this parameter (in fact the line intensity which is equivalent) was fitted
262 for each spectrum.

263 Final uncertainties on the spectroscopic parameters retrieved from the multi-spectrum fit
264 procedure at temperature T are then calculated as the square root of the quadratic sum of the type-
265 A and type-B errors. These 1σ -uncertainties are plotted in **Figure 3**. By looking to these plots, we can
266 observe that the estimated final uncertainties are consistent with the dispersion of the parameter
267 values, the fitted curves being within a $\pm 2\sigma$ interval in most of the cases. We nevertheless note that,
268 for some transitions, the final uncertainties seem to be underestimated by a factor of ~ 2 for the δ_0 ,
269 α_w and ζ parameters at 285 and 320 K and for the β parameter of the R(6) transition.

270 The uncertainties included in **Table 2** for the spectroscopic parameters at $T_{ref}= 296$ K and their
271 temperature dependence exponent, correspond to the fit error taking into account the uncertainties
272 on the spectroscopic parameters at each temperature.

273 4. Discussion

274 As mentioned above, a number of previous spectroscopic works have already been reported for
275 the $^{12}\text{CO}_2$ band studied here. We will limit our discussion to:

276 (i) The FTS measurements by Devi et al. [1] (also named hereafter Devi2016), whose results,
277 obtained with a quadratic speed-dependent Voigt profile including line-mixing, are implemented in
278 the latest version (5.1) of the absorption coefficient (ABSCO) tables for the Orbiting Carbon
279 Observatories for the 1.6 μm band [27],

280 (ii) The latest version of the HITRAN database (HITRAN2020) [16] which is based on empirical
281 modeling described in Ref. [18], adopting as in Ref. [1] a quadratic speed-dependent Voigt profile
282 with line-mixing,

283 (iii) The rCMDS calculations [19] (also named hereafter Nguyen2020) which provides Voigt
284 and non-Voigt line-shape parameters to complement the databases when no experimental data are
285 available. Note that the rCMDS spectroscopic parameters are only given for the P-branch, but
286 Nguyen et al. indicated that *the calculated R branch spectrum will be the exact symmetric of the P*
287 *branch* that we interpret as *the rCMDS spectroscopic parameters are function of the absolute value of*
288 *m where $m=-J$ and $J+1$ for the P- and R-branch, respectively* [19].

289 (iv) The Frequency-stabilized (FS)-CRDS measurements on the R(16) transition of the studied
290 band done at NIST between 240 and 290K using a SDNG profile (also named hereafter Ghysels2017)
291 [7].

292 Recently, several CRDS studies have reported highly accurate measurements (at the kHz level
293 or below) of the positions of the studied CO_2 transitions by saturation spectroscopy [6] or from
294 Doppler limited spectra [4,5]. The comparison of our fitted positions with the values provided by
295 these studies shows averaged differences (over the 5 transitions) from 25 kHz at 250K and 285 K, for
296 which the best signal-to-noise ratios are achieved, to 150 kHz in the worst case at 320 K. Fixing the
297 positions to these very accurate values during the multi-spectrum fit procedure modifies only
298 marginally the values retrieved for the different line-shape parameters.

299 a. Comparison of the air-broadening coefficients and their temperature dependence

300 Comparison of the retrieved air-broadening coefficients, $\gamma_0(T_{ref})$, with Devi et al, HITRAN and
301 rCMDS values is presented in the upper panel of **Figure 4**. As already observed in [18], rCMDS values
302 are systematically lower than measurements with differences of up to 2.6% compared to our values.
303 Let us remind, that in the rCMDS calculations, the molecules were considered as rigid rotors so that
304 all the effects of vibrational motion were disregarded. In fact, as shown in Fig. 6 of [28], the air-

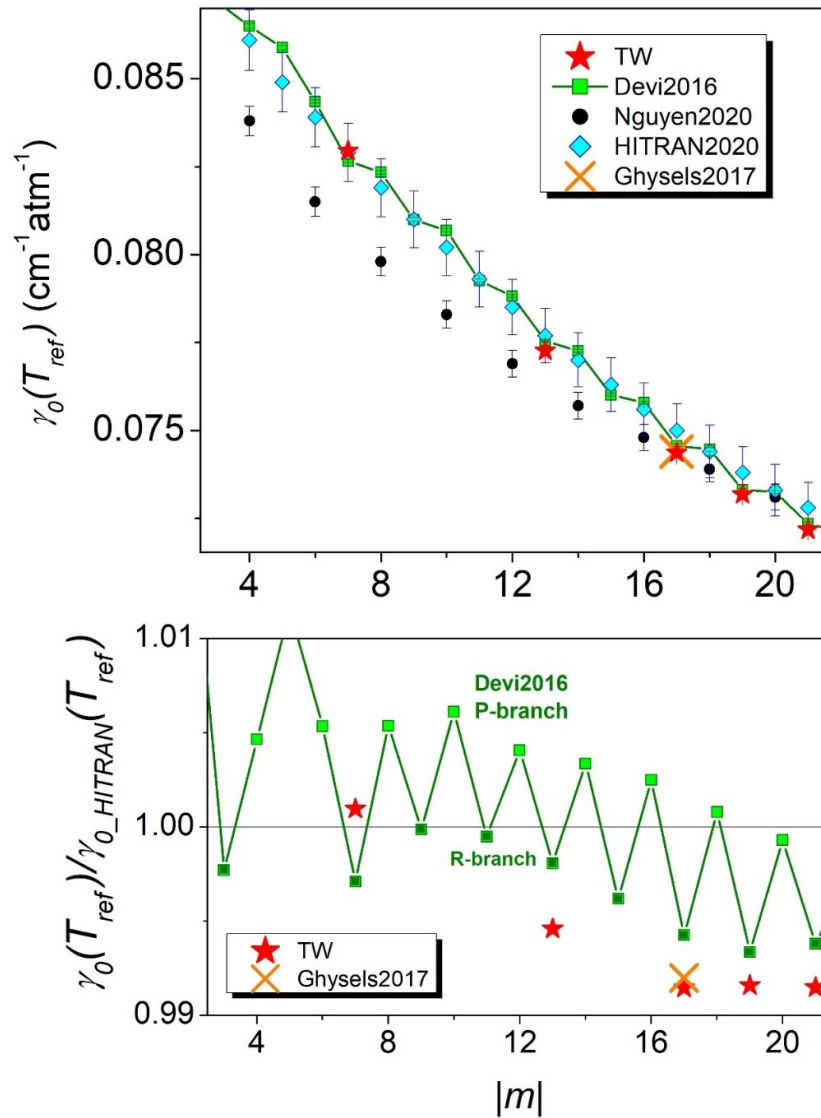
305 broadening coefficients at 296 K increase with the vibrational excitation up to few percent's. Due to
306 the underestimation of the rCMDS values, HITRAN2020 adopted rCMDS values for the air-broadening
307 coefficients of CO₂ [18] after a rescaling according to the FTS values of Devi et al.. In the lower panel
308 of **Figure 4**, we present the ratios of the experimental air-broadening coefficients to the
309 corresponding HITRAN2020 values. The agreement of our values with HITRAN2020 values is within
310 the HITRAN error bars (*i.e.* 1%) with differences from ~0.1% for R(6) line to 0.85% for the R(16), R(18)
311 and R(20) lines. Interestingly, a systematic difference by about 0.5 % is noted between the P- and R-
312 branches for the FTS values of Devi et al. This difference is between one and two orders of
313 magnitude larger than the experimental error bars of Devi et al. The same behavior is observed for
314 the 30012-00001 band from the data reported in [29]. If confirmed, it would indicate that a universal
315 law in $|m|$, as adopted in the HITRAN list for the air-broadening coefficients, is not adequate to
316 accurately account for the rotational dependence of the air-broadening coefficient in CO₂.

317 Air-broadening coefficients obtained in this work in the R-branch and by Devi et al. are close to
318 each other (**Figure 4**) with differences from -0.18% for the R(18) transition to +0.39% for the R(6)
319 transition. Nevertheless, for this latter transition, the particular FTS value seems to be ~0.3% smaller
320 than what could be extrapolated from the higher J lines of the R branch.

321 It is interesting to consider the impact of the line profile on the derived γ_0 values in particular
322 because Devi et al. adopted a SDV profile to model their FTS data while a SDNG profile was found
323 necessary to reproduce our CRDS spectra (see **Figure 2**). Following what has been done above to
324 quantify the temperature and pressure biases, we ran our fitting program with a SDV profile instead
325 of a SDNG profile. The γ_{0_SDV} fitted values were found systematically higher than our γ_{0_SDNG} values by
326 0.15 to 0.17%, thus compensating a significant part of the observed deviations (except for the R(6)
327 transition).

328 Another possible difference is related to the presence of argon in the air sample used for the
329 measurements. The dry air sample used by Devi et al corresponds to *Ultra Zero grade* from Airgas
330 which is a synthetic blend of 20-22% of oxygen and nitrogen, as found in the supplier documentation,
331 without 1% of argon contrary to our air sample. To evaluate the impact of argon, we used the results
332 of Ref. [29] where the O₂-, N₂- and Ar-broadening coefficients are measured for the nearby 30012-
333 00001 CO₂ band by frequency-agile rapid scanning (FARS) CRDS technique. Replacing 1% of N₂ by 1%
334 of Ar leads to a decrease of the broadening coefficient by ~0.2%. Note that the exact O₂ mixing ratio
335 in the mixture used by Devi et al. is not given and could also have an effect on the reported
336 broadening coefficients.

337 After correction of the FTS data from these two effects, the differences are reduced to less than
338 0.2% for the R(10), R(16), R(18) and R(20) transitions, the deviation of the R(6) "outlier" reaching a
339 value of 0.7%.



341

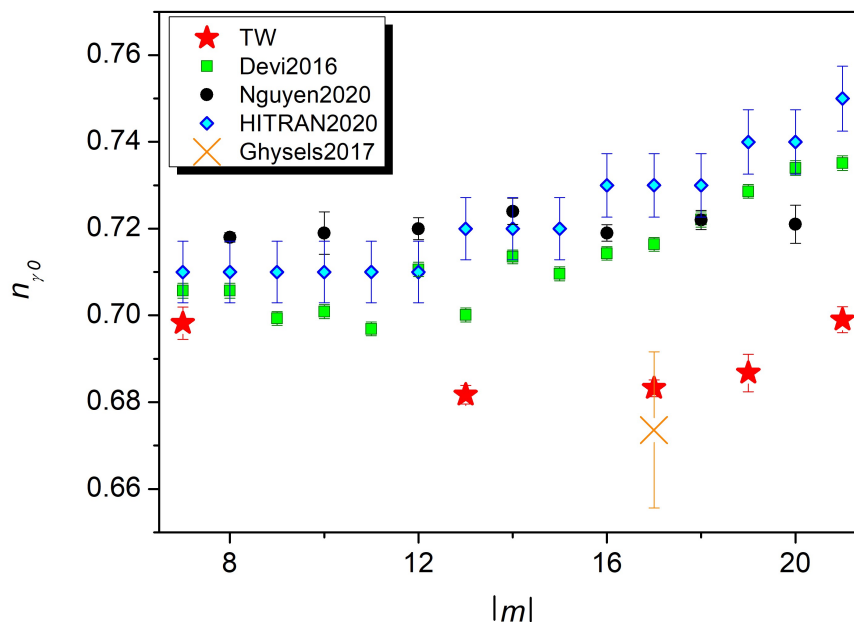
342

343 *Figure 4. Comparison of the retrieved air-broadening coefficients, $\gamma_0(T_{ref})$, with a selection of recent works:*344 *Devi2016 [1], Nguyen2020 [19], Ghysels2017 [7] and HITRAN2020 [16] (Upper panel). Ratios of the air-*345 *broadening coefficients obtained in this work (TW), in Devi2016 and in Ghysels2017 to those of HITRAN2020 are*346 *presented in the lower panel. A 1%-uncertainty is reported for HITRAN2020 values. Note the weak asymmetric*347 *behavior between the P- and R-branch.*348 We have included in Fig. 4, the NIST value for the R(16) transition [7] obtained for 400 ppm of CO_2

349 in purified dry air (thus containing argon as in our sample) using a SDNG profile. An excellent

350 agreement is achieved (difference of about 0.04%).

351 From this discussion, we conclude that accuracy on the γ_0 determination at the 0.1% level
 352 requires to carefully consider the impact of the line profile and the composition of the dry air sample
 353 (fraction of O₂ and N₂, presence of argon).



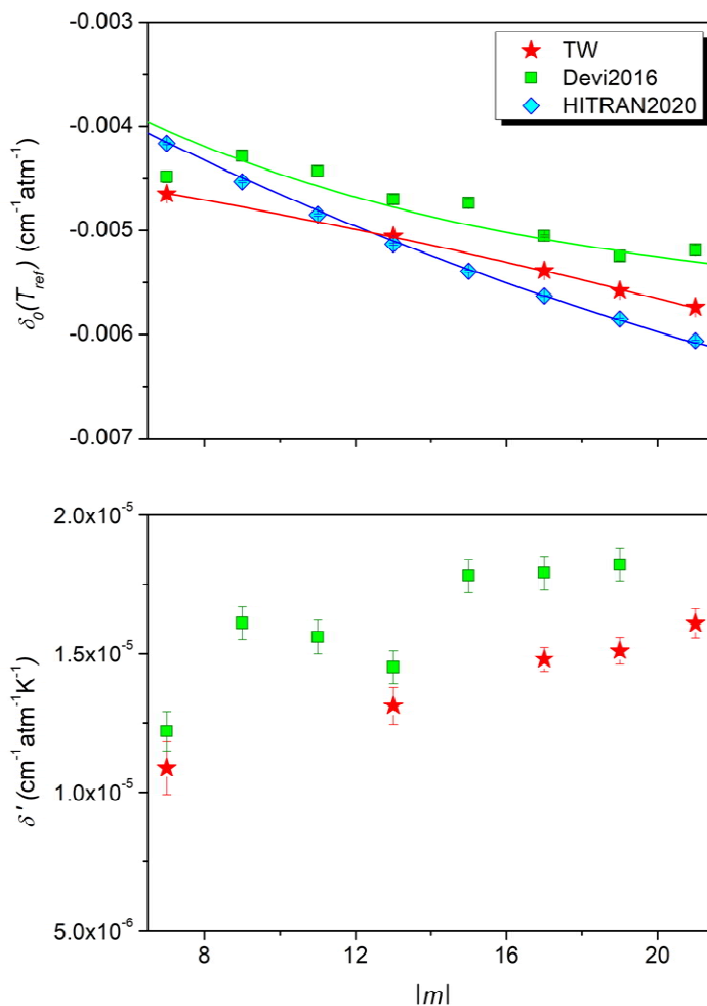
354
 355 *Figure 5. Comparison of the retrieved temperature dependence exponent of the air-broadening coefficient,*
 356 *n_{γ_0} , with a selection of recent works: Devi2016 [1], Nguyen2020 [19], Ghysels2017 [7] and HITRAN2020 [16].*

357 The γ_0 temperature dependence exponent obtained in the present work shows a clear m
 358 dependence contrary to the rCMDS calculated values which are almost constant for $|m| > 5$ (see **Fig.**
 359 **5**). The rCMDS values are systematically higher by 2.5 to 6% which can be considered as satisfactory
 360 for these calculations [19]. The comparison with Devi et al gives differences on the same order. As
 361 rCMDS calculations of n_{γ_0} for air and O₂ show that n_{γ_0} is not very sensitive to the perturber [19], the
 362 observed deviations cannot be due to the presence of 1% of argon in our air mixture. The observed
 363 differences are possibly explained by the use of different line profiles (*i.e.* SDNG profile in this work
 364 and a SDV profile in Devi et al.).

365 For the R(16) transition we see that the NIST n_{γ_0} value [7] obtained with a SDNG profile agrees
 366 with our value. In the same paper, the n_{γ_0} value retrieved from a SDV profile was found in very good
 367 agreement with the value reported in Devi et al. which might indicate that temperature dependence
 368 exponent of the air-broadening coefficient is quite sensitive to the choice of the profile. The fitting of
 369 our spectra with a SDV profile did not confirm this sensitivity, the retrieved n_{γ_0} value being almost
 370 unchanged when using one or the other profile (including line-mixing effects). Note that NIST
 371 estimated uncertainty of 0.018 is about ten times larger than what is estimated for the same

372 transition in our work (0.002). If we try to fit our $\gamma_0(T)$ data by fixing n_{γ_0} to the values reported by Devi
 373 et al. (and by freeing $\gamma_0(T_{ref})$), a clear mismatch between the fit and our data is observed with
 374 differences up to $\pm 0.4\%$ for the two “extreme” temperatures (250 and 320 K). This shows the
 375 importance of an accurate determination of n_{γ_0} . As HITRAN2020 values are fitted on the FTS data of
 376 Devi et al. with Padé approximants, similar differences are observed compared to HITRAN values.

377 *b. Comparison of the air-pressure shifts and their temperature dependence*

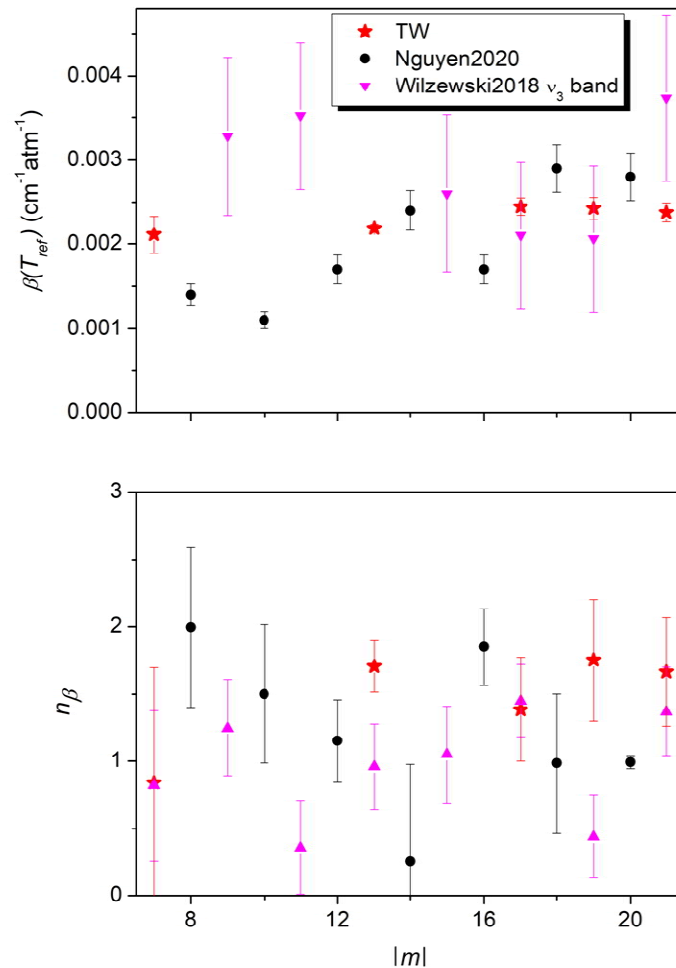


378
 379 *Figure 6. Comparison of the retrieved air-pressure shift coefficients, $\delta_0(T_{ref})$, (Upper panel) and its*
 380 *temperature dependence coefficients, δ' , with Devi2016 [1] and HITRAN2020 [16]. Note that no temperature*
 381 *dependence is reported in HITRAN2020.*

382 In HITRAN2020, the approach proposed by Hartmann [30] is adopted to extend to other
 383 vibrational bands the air-pressure shift coefficients fitted to one band. The good agreement observed
 384 with our data (**Figure 6**) demonstrates the relevance of this approach. Devi et al. pressure shifts are
 385 smaller than our values by amounts between 3×10^{-4} and $5.5 \times 10^{-4} \text{ cm}^{-1} \text{atm}^{-1}$ which are outside the

386 combined error bars. But, the reported FTS error bars (typ. $4.5 \times 10^{-5} \text{ cm}^{-1} \text{ atm}^{-1}$) do not include
 387 systematic uncertainties due to wavenumber calibration of the spectra and physical conditions of the
 388 spectra. Let us note here that the wavenumber calibration of the FTS spectra recorded by Devi et al
 389 was performed using additional absorption cells containing gases (CO, C₂H₂ or HCl) for which some
 390 transitions have accurately known positions, so that the overall FTS absolute uncertainty on line
 391 positions was estimated to be better than $\pm 0.0001 \text{ cm}^{-1}$. This uncertainty is a factor of 20 larger than
 392 the worst uncertainty on the absolute value of our fitted line positions. Our pressure-shift
 393 temperature dependence coefficients are close to the FTS values (although outside the combined
 394 error bars) and show an overall smooth increase with $|m|$ (lower panel of **Figure 6**).

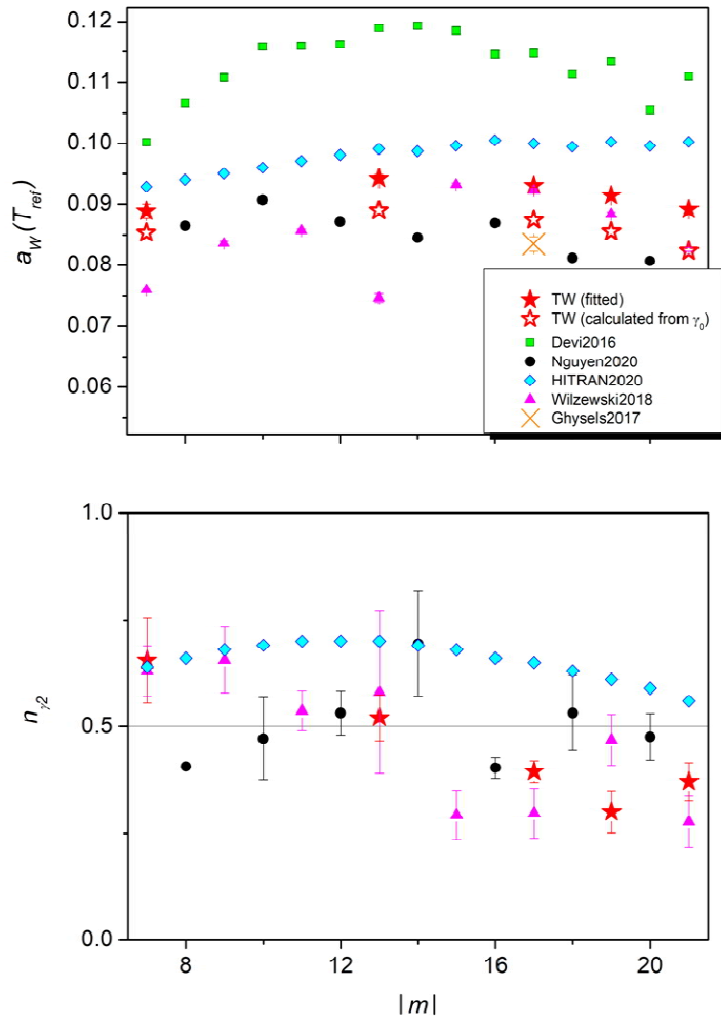
395 *c. Comparison of the Dicke narrowing parameters*



396
 397 *Figure 7. Comparison of the retrieved Dicke narrowing coefficients, $\beta(T_{ref})$, and of its temperature*
 398 *dependence exponent, n_β , with a selection of recent works: Nguyen2020 [19] and Wilzewski2018 [31].*

399 As expected, no evident m dependence is observed for β and n_β (**Figure 7**). With a weighted mean
 400 value over m of $0.00230(18) \text{ cm}^{-1}\text{atm}^{-1}$, our Dicke narrowing coefficients are found in good
 401 agreement with SDNGP values obtained in Wilzewski2018 [31] for the ν_3 band of $^{12}\text{CO}_2$ in N_2 and with
 402 the rCMDS values [19] (for CO_2 in air). Note that these values are quite different from the value of
 403 $0.0199 \text{ cm}^{-1}\text{atm}^{-1}$ obtained from the diffusion coefficient of CO_2 in air derived from the kinetic theory
 404 of gases [26,32]. The retrieved temperature dependence exponents of the Dicke narrowing
 405 coefficients, n_β , are not accurately determined neither by experiment nor by rCMDS calculations
 406 (**Figure 7**) but the different values roughly agree within their large error bars. In our case, the
 407 weighted mean value of n_β is 1.45 ± 0.32 .

408 *d. The speed-dependent parameters and their temperature dependence*



409
 410 *Figure 8. Comparison of the speed dependent parameter, $a_w(T_{ref})$, and of its temperature dependence*
 411 *exponent, n_{γ_2} , with a selection of recent works: Devi2016 [1], Nguyen2020 [19], Ghysels2017 [7],*
 412 *Wilzewski2018 [31] and HITRAN2020 [16].*

413 The $|m|$ dependence of the speed dependent broadening parameter, $a_w(T_{ref})$, is presented in
414 **Figure 8** together with selected literature data. According to Ref. [33], the $a_w(T_{ref})$ values can be
415 computed from the retrieved $\gamma_0(T)$ broadening coefficients and the m_p/m_a mass ratio where m_p and
416 m_a correspond to the mass of the perturber and of the absorber, respectively. The obtained values,
417 included in **Figure 8**, are found consistent with our $a_w(T_{ref})$ values although systematically smaller by
418 5-7%. Our values are also in good agreement with the rCMDS and HITRAN2020 data and the
419 experimental values of Wilzewski et al. [31] based on a quadratic SDNG profile. Note that the latter
420 study concerns the ν_3 band of CO_2 in N_2 and not in air. But, by using Ref. [33] to calculate $a_w(T)$, we
421 see that replacing air by N_2 decreases $a_w(T_{ref})$ by only 2% for the R(20) transition for example. The a_w
422 value reported by NIST for the R(16) transition is 11.5% lower than our value but this could be
423 explained by the fact that a_w was considered as independent of the temperature [7].

424 The FTS values of Devi et al. are notably larger than other experimental sources by about 25%.
425 This difference should only be partially explained by the use of a SDV profile instead of a SDNG
426 profile in our work. Indeed, simulations based on the MATS program, indicate that, in our conditions,
427 replacing the SDNG profile by a SDV one, leads to an increase of a_w by 5 to 6%. The agreement of
428 Devi et al. is also not very good with the HITRAN2020 data derived from rCMDS using a SDV profile.
429 The difference may also be related to the fact that Devi et al. assumed that a_w is identical for both
430 self- and air-broadening and independent of the gas sample temperature ($n_{\gamma_2} = 1$). This latter
431 assumption is in contradiction with both our results and the experimental results reported by
432 Wilzewski et al. for the ν_3 band (with n_{γ_2} on the order of 0.5) (**Figure 8**).

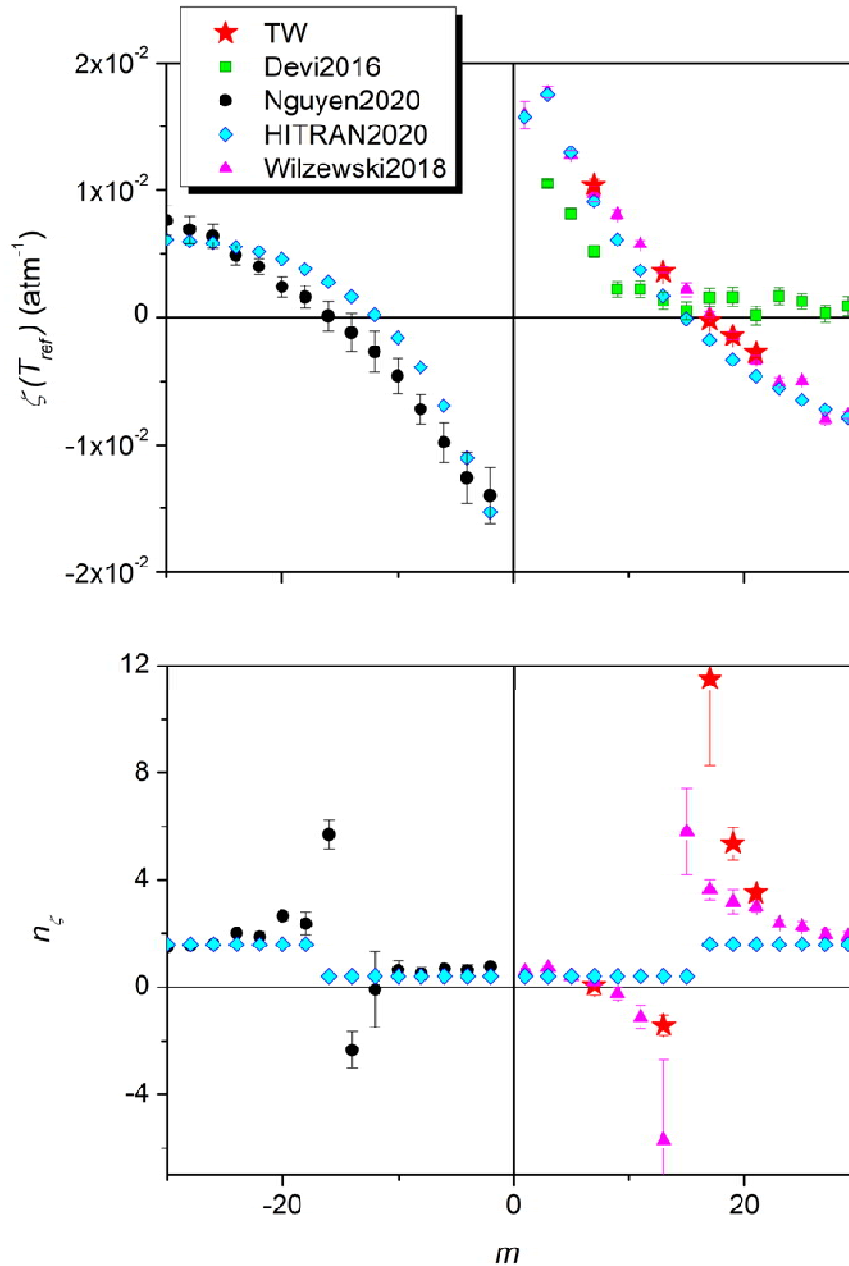
433 The rCMDS and HITRAN2020 n_{γ_2} values (derived from rCMDS calculations fitted with a SDV
434 profile) are in rough agreement with the experimental data. Note that our data and those of
435 Wilzewski et al. seem to show a slow decrease with $|m|$ contrary to rCMDS and HITRAN2020 data.

436 To our knowledge, no data are available for comparison of a_s (**Table 2**) for which no temperature
437 dependence is detected. A clear decrease with m from 0.093 to 0.053 for $m= 7$ to 21 is obtained for
438 the values averaged over the five temperatures of our measurements.

439 *e. The line-mixing parameters and their temperature dependence*

440 Our first-order line mixing parameters at 296 K are plotted on **Figure 9** together with the rCMDS,
441 HITRAN2020 values and the ν_3 results of [31]. The experimental values (relative to different bands)
442 are in close coincidence indicating that there is almost no vibrational dependence. This is confirmed
443 by the rCMDS results (with no vibrational dependence considered) which are systematically smaller
444 but agree satisfactorily with both experimental datasets. The same satisfactory agreement is
445 observed with HITRAN2020 values calculated by Lamouroux et al. [34] using the Energy-Corrected
446 Sudden (ECS) approximation.

447 Devi et al. reported off-diagonal relaxation matrix element coefficients between the nearest
448 neighbor pairs. To convert these matrix element coefficients into the line-mixing parameters plotted
449 on **Figure 9**, we used Eq. IV.24 of [35] and Eq. 7 of [36]. The m dependence reported by Devi et al.
450 differs noticeably compared to the experimental values. Devi et al mentioned that *the values of these*
451 *line mixing temperature dependence exponents (...) showed no systematic variations with m or J*
452 *contrary to what is shown on **Figure 9**, where the CRDS, FTS and rCMDS temperature dependence*
453 *exponents, n_ζ , are all in good agreement, showing a clear dependence with m with a rapid variation*
454 *near $m= 15$. To simplify the calculations with HAPI [37], two average values over m were adopted for*
455 *in HITRAN2020 with $n_\zeta = 0.41$ for $m \leq 16$ and $n_\zeta = 1.6$ for $m > 16$ [18].*



456

457 *Figure 9. Comparison of the line-mixing parameter, $\zeta(T_{ref})$, and of its temperature dependence exponent, n_{ζ} ,*
 458 *with a selection of recent works: Devi2016 [1], Nguyen2020 [19], Wilzewski2018 [31] and HITRAN2020 [16].*

459

5. Conclusion

460

461 Line-shapes of five transitions of the 30013-00001 band of carbon dioxide have been studied from
 462 high sensitivity CRDS spectra recorded with the help of a narrowed and stable (sub-kHz) laser source.
 463 Series of spectra were recorded in different conditions of temperature (from 250 to 320 K) and
 464 pressure (from 50 to 750 Torr) for a mixture of ~ 400 ppm of CO_2 in air. From a multi-spectrum fit
 procedure using quadratic SDNG profiles, including the line-mixing effects, the line-shape parameters

465 were retrieved with reduced uncertainties and limited numerical correlations. Temperature
466 dependence is reported for all of these parameters. Noticeably, contrary to what was claimed in
467 some previous works, a clear temperature dependence is noticed for the speed dependence
468 component of the air-broadening coefficient, very similar to what has been observed in Wilzewski et
469 al. for the ν_3 band of CO_2 . No temperature dependence is observed for the speed dependence
470 component of the air pressure-shift coefficient. A good overall agreement is obtained with rCMDS
471 data for the different parameters, which participates to the validation of these calculations aiming to
472 fill the databases for the non-Voigt spectroscopic parameters.

473 A comparison with HITRAN2020 shows that the values reported in this database for the air
474 pressure-broadening and -shift coefficients of the studied transitions are in good agreements with
475 our values. An agreement better than 0.2% is found between the air-pressure-broadening
476 coefficients obtained at 296 K in this work and those from Devi et al., used in the ABSCO tables for
477 the OCO missions, for four of the five transitions studied. Nevertheless, the temperature dependence
478 exponents in Devi et al are systematically higher by up to 6% leading to differences close to 1% for γ_0
479 at the lowest atmospheric temperatures. Interestingly, the comparison of our results to the air
480 pressure-broadening available in the literature, in particular the FTS values of Devi et al. and the
481 CRDS values of Adkins et al. [29], revealed a systematic difference by about 0.5 % between the P- and
482 R- branches (**Fig. 4** bottom panel), largely above the experimental uncertainty. The origin of this
483 effect which was apparently not noted in Refs. [1,29], remains unclear but may indicate that the
484 universal law in $|m|$, as adopted in the HITRAN list for the air-broadening coefficients, is not
485 adequate to account for the rotational dependence of the air-broadening coefficient in CO_2 at the
486 level of accuracy achieved by the best experiments. Different empirical laws for the P- and R-
487 branches might be required.

488

489 **Acknowledgements**

490 This work is funded by the European Space Agency (ESA) through the contract No.
491 4000132228/20/I-NS with Deutsches Zentrum fuer Luft- und Raumfahrt) entitled *Improved*
492 *Spectroscopy for Carbon Dioxide, Oxygen, and Water Vapour Satellite Measurements* for which the
493 authors are sub-contractants. DM wants to thank H. Tran for fruitful discussions on rCMDS results.

494

- [1] Devi VM, Benner DC, Sung K, Brown LR, Crawford TJ, Miller CE, Drouin BJ, Payne VH, Yu S, Smith MAH, Mantz AW, Gamache RR. Line parameters including temperature dependences of self- and air-broadened line shapes of $^{12}\text{C}^{16}\text{O}_2$: 1.6- μm region. *J Quant Spectrosc Radiat Transf* 2016;177:117-144. Doi: 10.1016/j.jqsrt.2015.12.020.
- [2] Birk M, Röske C, Wagner G. High accuracy CO_2 Fourier transform measurements in the range 6000–7000 cm^{-1} . *J Quant Spectrosc Radiat Transf* 2021;272:107791. Doi: 10.1016/j.jqsrt.2021.107791.
- [3] Long DA, Truong G-W, Hodges JT, Miller CE. Absolute $^{12}\text{C}^{16}\text{O}_2$ transition frequencies at the kHz-level from 1.6 to 7.8 μm . *J Quant Spectrosc Radiat Transf* 2013;130:112-115. Doi : 10.1016/j.jqsrt.2013.07.001.
- [4] Reed ZD, Drouin BJ, Long DA, Hodges JT. Molecular transition frequencies of CO_2 near 1.6 μm with kHz-level uncertainties. *J Quant Spectrosc Radiat Transf* 2021; 271:107681. Doi : 10.1016/j.jqsrt.2021.107681.
- [5] Reed ZD, Drouin BJ, Hodges JT. Inclusion of the recoil shift in Doppler-broadened measurements of CO_2 transition frequencies. *J Quant Spectrosc Radiat Transf* 2021; 275:107885. Doi : 10.1016/j.jqsrt.2021.107885.
- [6] Wu H, Hu C-L, Wang J, Sun YR, Tan Y, Liu A-W, Hu S-M. A well-isolated vibrational state of CO_2 verified by near-infrared saturated spectroscopy with kHz accuracy. *Phys Chem Chem Phys* 2020;22:2841-2848. Doi: 10.1039/C9CP05121J
- [7] Ghysels M, Liu Q, Fleisher AJ, Hodges JT. A variable-temperature cavity ring-down spectrometer with application to line shape analysis of CO_2 spectra in the 1600 nm region. *Appl Phys B* 2017;123:124. Doi :10.1007/s00340-017-6686-y
- [8] Crisp D, Atlas RM, Breon F-M, Brown LR, Burrows JP, Ciais P, Connor BJ, Doney SC, Fung IY, Jacob DJ, Miller CE, O'Brien D, Pawson S, Randerson JT, Rayner P, Salawitch RJ, Sander SP, Sen B, Stephens GL, Tans PP, Toon GC, Wennberg PO, Wofsy SC, Yung YL, Kuang Z, Chudasama B, Sprague G, Weiss B, Pollock R, Kenyon D, Schroll S. The Orbiting Carbon Observatory (OCO) mission. *Adv Space Res* 2004;34:700–709. Doi: 10.1016/j.asr.2003.08.062.
- [9] Crisp D, Miller CE, DeCola PL. NASA Orbiting Carbon Observatory: measuring the column averaged carbon dioxide mole fraction from space. *J Appl Rem Sens* 2008;2:023508. Doi: 10.1117/ 1.2898457.
- [10] Boesch H, Baker D, Connor B, Crisp D, Miller CE. Global characterization of CO_2 column retrievals from shortwave-infrared satellite observations of the Orbiting Carbon Obs-2 Mission. *Remote Sens* 2011;3:270–304. Doi: 10.3390/rs3020270
- [11] Eldering A, Taylor TE, O'Dell CW, PavlickR. The OCO-3 mission: measurement objectives and expected performance based on 1 year of simulated data. *Atmos Meas Tech* 2019;12:2341–2370. Doi: 10.5194/amt-12-2341-2019.
- [12] Kuze A, Suto H, Nakajima M, Hamazaki T. Thermal and near infrared sensor for carbon observation Fourier transform spectrometer on the Greenhouse Gases Observing Satellite for greenhouse gases monitoring. *Appl Opt* 2009;48:6716–33. Doi:10.1364/AO.48.006716.
- [13] Miller CE, Crisp D, DeCola PL, Olsen SC, Randerson JT, Michalak AM, Alkhaled A, Rayner P, Jacob DJ, Suntharalingam P, Jones DBA, Denning AS, Nicholls ME, Doney SC, Pawson S, Boesch H, Connor BJ, Fung IY, O'Brien D, Salawitch RJ, Sander SP, Sen B, Tans P, Toon GC, Wennberg PO, Wofsy SC, Yung YL, Law RM. Precision requirements for space-based X_{CO_2} data. *J Geophys Res: Atmos* 2007;112:D10314. Doi:10.1029/2006JD007659
- [14] Hobbs JM, Drouin BJ, Oyafuso F, Payne VH, Gunson MR, McDuffie J, Mlawer EJ. Spectroscopic uncertainty impacts on OCO-2/3 retrievals of X_{CO_2} . *J Quant Spectrosc Radiat Transf* 2020;257:107360. Doi: 10.1016/j.jqsrt.2020.107360.
- [15] Copernicus CO_2 Monitoring Mission Requirements Document, EOP-SM/3088/YM-ymIssue 2.0, 2019. available via https://esamultimedia.esa.int/docs/EarthObservation/CO2M_MRD_v2.0_Issued20190927.pdf
- [16] Gordon IE, Rothman LS, Hargreaves RJ, Hashemi R, Karlovets EV, Skinner FM, Conway EK, Hill C, Kochanov RV, Tan Y, Wcislo P, Finenko AA, Nelson K, Bernath PF, Birk M, Boudon V, Campargue A, Chance KV, Coustenis A, Drouin BJ, Flaud J-M, Gamache RR, Hodges JT, Jacquemart D, Mlawer EJ, Nikitin AV, Perevalov VI, Rotger M, Tennyson J, Toon GC, Tran H, Tyuterev VG, Adkins EM, Baker A, Barbe A, Canè E, Császár AG, Dudaryonok A, Egorov O, Fleisher AJ, Fleurbaey H, Foltynowicz A, Furtenbacher T, Harrison JJ, Hartmann J-M, Horneman V-M, Huang X, Karman T, Karns J, Kassi S, Kleiner I, Kofman V, Kwabia-Tchana F, Lavrentieva NN, Lee TJ, Long DA, Lukasheskaya AA, Lyulin OM, Makhnev VY, Matt W, Massie ST, Melosso M, Mikhailenko SN, Mondelain D, Müller HSP, Naumenko OV, Perrin A, Polyansky OL, Raddaoui E, Raston PL, Reed ZD, Rey M, Richard C, Tóbiás R, Sadiq I, Schwenke DW, Starikova E, Sung K, Tamassia F, Tashkun SA, Vander Auwera J, Vasilenko IA, Vigasin

-
- AA, Villanueva GL, Vispoel B, Wagner G, Yachmenev A, Yurchenko SN. The HITRAN2020 molecular spectroscopic database. *J Quant Spectrosc Radiat Transf* 2022; 277:107949. Doi: 10.1016/j.jqsrt.2021.107949.
- [17] Jacquinet-Husson N, Armante R, Scott NA, Chédin A, Crépeau L, Boutammine C, Bouhdaoui A, Crevoisier C, Capelle V, Boone C, Poulet-Crovisier N, Barbe A, Benner DC, Boudon V, Brown LR, Buldyreva J, Campargue A, Coudert LH, Devi VM, Down MJ, Drouin BJ, Fayt A, Fittschen C, Flaud J-M, Gamache RR, Harrison JJ, Hill C, Hodnebrog Ø, Hu S-M, Jacquemart D, Jolly A, Jiménez E, Lavrentieva NN, Liu A-W, Lodi L, Lyulin OM, Massie ST, Mikhailenko S, Müller HSP, Naumenko OV, Nikitin A, Nielsen CJ, Orphal J, Perevalov VI, Perrin A, Polovtseva E, Predoi-Cross A, Rotger M, Ruth AA, Yu SS, Sung K, Tashkun SA, Tennyson J, Tyuterev VG, Vander Auwera J, Voronin BA, Makie A. The 2015 edition of the GEISA spectroscopic database, *J Mol Spectr* 2016; 327:31-72. Doi : 10.1016/j.jms.2016.06.007.
- [18] Hashemi R, Gordon IE, Tran H, Kochanov RV, Karlovets EV, Tan Y, Lamouroux J, Ngo NH, Rothman LS. Revising the line-shape parameters for air- and self broadened CO₂ lines toward a sub-percent accuracy level, *J Quant Spectrosc Radiat Transf* 2020;256:107283. Doi: 10.1016/j.jqsrt.2020.107283.
- [19] Nguyen HT, Ngo NH, Tran H. Line-shape parameters and their temperature dependences predicted from molecular dynamics simulations for O₂- and air-broadened CO₂ lines. *J Quant Spectrosc Radiat Transf* 2020;242:106729. Doi: 10.1016/j.jqsrt.2019.106729.
- [20] Vasilchenko S, Delahaye T, Kassi S, Campargue A, Tran H, Mondelain D. Temperature dependence of the absorption of the R(6) manifold of the 2v₃ band of methane in air for the MERLIN mission. Submitted to JQSRT.
- [21] Burkart J, Romanini D, Kassi S. Optical feedback stabilized laser tuned by single-sideband modulation. *Opt Lett* 2013;38:2062-2064. Doi:
- [22] Kassi S, Guessoum S, Abanto JCA, Tran H, Campargue A, Mondelain D. Temperature dependence of the collision-induced absorption band of O₂ near 1.27 μm. *J Geophys Res Atm* 2021;126:e2021JD034860. Doi : 10.1029/2021JD034860.
- [23] <https://github.com/usnistgov/MATS>. Doi:10.18434/M32200
- [24] Tran H, Ngo NH, Hartmann J-M. Efficient computation of some speed-dependent isolated line profiles. *J Quant Spectrosc Radiat Transf* 2013;129:199-20. Doi :10.1016/j.jqsrt.2013.06.015.
- [25] Rosenkranz PK. Shape of the 5 μm oxygen band in the atmosphere. *IEEE Trans Antennas Propag* 1975;23:498–506.
- [26] Adkins EM, Hodges JT. Assessment of the precision, bias and numerical correlation of fitted parameters obtained by multi-spectrum fits of the Hartmann-Tran line profile to simulated absorption spectra, *J Quant Spectrosc Radiat Transf* 2022;280:108100. Doi: 10.1016/j.jqsrt.2022.108100.
- [27] Payne VH, Drouin BJ, Oyafuso F, Kuai L, Fisher BM, Sung K, Nemchick D, Crawford TJ, Smyth M, Crisp D, Adkins E, Hodges JT, Long DA, Mlawer EJ, Merrelli A, Lunny E, O'Dell CW. Absorption coefficient (ABSCO) tables for the Orbiting Carbon Observatories: Version 5.1. *J Quant Spectrosc Radiat Transf* 2020;255:107217. Doi : 10.1016/j.jqsrt.2020.107217.
- [28] Gamache RR, Lamouroux J. The vibrational dependence of half-widths of CO₂ transitions broadened by N₂, O₂, air, and CO₂. *J Quant Spectrosc Radiat Transf* 2013;117:93-103. Doi: 10.1016/j.jqsrt.2012.10.028.
- [29] Adkins EM, Long DA, Hodges JT. Air-broadening in near-infrared carbon dioxide line shapes: Quantifying contributions from O₂, N₂, and Ar. *J Quant Spectrosc Radiat Transf* 2021;270:107669. Doi: 10.1016/j.jqsrt.2021.107669.
- [30] Hartmann J-M. A simple empirical model for the collisional spectral shift of air-broadened CO₂ lines. *J Quant Spectrosc Radiat Transfer* 2009;110(18):2019–2026. Doi:10.1016/j.jqsrt.2009.05.016
- [31] Wilzewski JS, Birk M, Loos J, Wagner G. Temperature-dependence laws of absorption line shape parameters of the CO₂ v₃ band. *J Quant Spectrosc Radiat Transf* 2018;206:296-305. Doi: 10.1016/j.jqsrt.2017.11.021.
- [32] <https://demonstrations.wolfram.com/BinaryDiffusionCoefficientsForGases/>
- [33] Lisak D, Cygan A, Wcisło P, Ciuryło R. Quadratic speed dependence of collisional broadening and shifting for atmospheric applications. *J Quant Spectrosc Radiat Transf* 2015; 151:43-48. Doi : 10.1016/j.jqsrt.2014.08.016.
- [34] Lamouroux J, Régalia L, Thomas X, Auwera JV, Gamache R, Hartmann J-M. CO₂ line-mixing database and software update and its tests in the 2.1 μm and 4.3 μm regions. *J Quant Spectrosc Radiat Transfer* 2015;151:88–96. Doi:10.1016/j.jqsrt.2014.09.017.
- [35] Hartmann J-M, Boulet C, Robert D, Chapter IV - Collisional line mixing (within clusters of lines), Editor(s): J-M Hartmann, C Boulet, D Robert, *Collisional Effects on Molecular Spectra (Second Edition)*, Elsevier, 2021, Pages 181-289. Doi : 10.1016/B978-0-12-822364-2.00004-0.
- [36] Tran H, Flaud J-M, Gabard T, Hase F, von Clarmann T, Camy-Peyret C, Payan S, Hartmann J-M.

Model, software and database for line-mixing effects in the ν_3 and ν_4 bands of CH_4 and tests using laboratory and planetary measurements—I: N_2 (and air) broadenings and the earth atmosphere. *J Quant Spectrosc Radiat Transf* 2006;101:284-305. Doi: 10.1016/j.jqsrt.2005.11.020.

[37] Kochanov RV, Gordon IE, Rothman LS, Wcislo P, Hill C, Wilzewski JS. HITRAN Application Programming Interface (HAPI): A comprehensive approach to working with spectroscopic data *J Quant Spectrosc Radiat Transfer* 2016;177:15-30. Doi : 10.1016/j.jqsrt.2016.03.005